

## Robust deep identification using ECG and multimodal biometrics for industrial internet of things

Item Type	Journal article
Authors	Alkeem, Ebrahim Al;Yeob Yeun, Chan;Yun, Jaewoong;Yoo, Paul D;Chae, Myungsu;Rahman, Arafatur;Asyhari, A. Taufiq
Citation	Alkeem, EA, Yeun, CY, Yun, J, Yoo, P D, et al (2021) Robust Deep Identification using ECG and Multimodal Biometrics for Industrial Internet of Things, Ad Hoc Networks, 121, Article Number 102581
DOI	<a href="https://doi.org/10.1016/j.adhoc.2021.102581">10.1016/j.adhoc.2021.102581</a>
Publisher	Elsevier
Journal	Ad Hoc Networks
Download date	2026-04-18 06:28:05
License	<a href="https://creativecommons.org/licenses/by-nc-nd/4.0/">https://creativecommons.org/licenses/by-nc-nd/4.0/</a>
Link to Item	<a href="http://hdl.handle.net/2436/624222">http://hdl.handle.net/2436/624222</a>

# Robust Deep Identification using ECG and Multimodal Biometrics for Industrial Internet of Things

Ebrahim Al Alkeem<sup>1,2</sup>, Chan Yeob Yeun<sup>1</sup>, Jaewoong Yun<sup>3</sup>, Paul D. Yoo<sup>4</sup>, Myungsu Chae<sup>3</sup>, Arafatur Rahman<sup>5</sup> and A. Taufiq Asyhari<sup>6</sup>

<sup>1</sup>Center for Cyber-Physical Systems, EECS Department, Khalifa University, Abu Dhabi, UAE

<sup>2</sup>Security and Safety, Nawah Energy Company, Abu Dhabi, UAE

<sup>3</sup>Research Institute NOTA Incorporated, Daejeon, South Korea

<sup>4</sup>CSIS, Birkbeck College, University of London, Malet Street, London, WC1E 7HX, United Kingdom

<sup>5</sup>School of Mathematics and Computer Science, University of Wolverhampton, Wulfruna St, Wolverhampton WV1 1LY, UK.

<sup>6</sup>CDT, Birmingham City University, Millennium Point, Birmingham, B4 7XG, United Kingdom

\*Correspondence: [chan.yeun@ku.ac.ae](mailto:chan.yeun@ku.ac.ae)

**Abstract:** The use of electrocardiogram (ECG) data for personal identification in Industrial Internet of Things can achieve near-perfect accuracy in an ideal condition. However, real-life ECG data are often exposed to various types of noises and interferences. A reliable and enhanced identification method could be achieved by employing additional features from other biometric sources. This work, thus, proposes a novel robust and reliable identification technique grounded on multimodal biometrics, which utilizes deep learning to combine fingerprint, ECG and facial image data, particularly useful for identification and gender classification purposes. The multimodal approach allows the model to deal with a range of input domains removing the requirement of independent training on each modality, and inter-domain correlation can improve the model generalization capability on these tasks. In multitask learning, losses from one task help to regularize others, thus, leading to better overall performances. The proposed approach merges the embedding of multimodality by using feature-level and score level fusions. To the best of our understanding, the key concepts presented herein is a pioneering work combining multimodality, multitasking and different fusion methods. The proposed model achieves a better generalization on the benchmark dataset used while the feature-level fusion outperforms other fusion methods. The proposed model is validated on noisy and incomplete data with missing modalities and the analyses on the experimental results are provided.

**Keywords:** Personal identification; multimodal biometrics; deep learning; gender classification; electrocardiogram; fingerprint; face recognition; feature-level fusion

## 1. Introduction

Personal identification using electrocardiogram (ECG) data is a recent development in biometrics and has a great potential to be applied in Industrial Internet of Things (IIoT) environments. Such system presented with ECG data can return identifications by verifying whether or not individuals are in the database. Previous researches have focused on identification and authentication using databases of ECG profiles acquired from only a few subjects under restricted conditions [1–11]. However, ECGs captured in real-life are likely to contain noises and interferences, requiring the identification based on unseen ECG profiles to be robust towards noisy and incomplete data.

Traditional machine learning (ML) methods for personal identification include feature extraction and classification methods, but deep learning (DL) approaches can achieve better results

47 for several reasons. First, ML methods are generally comprised of a channel of tailored feature  
48 extraction and classification techniques, such as k-nearest neighbors (kNN) or random forest,  
49 resulting in uncertainty of being able to extract solely informative features. Performances are  
50 determined by the selected combination of feature extraction and classification methods, which may  
51 lead to poor performances. In contrast, the DL utilizes neurons, which broaden the choice of feature  
52 extraction and learning models. This degree of freedom means that modeling between raw data and  
53 the label is trained by the gradient descent rule, which minimizes overall losses.

54 Second, the DL is superficial with structured raw data (e.g., audio and image data), whereas the  
55 hand-crafted features captured by the ML may also contain unrelated features. If the input is less  
56 structured (e.g., age or gender) then feature extraction is unnecessary. However, image and audio  
57 data are highly dimensional, so feature extraction should be considered carefully. DLs outperform  
58 MLs on image and audio data in various domains [12, 13].

59 Third, the DL is typically preferred for the analysis of ECG data [14–16]. For example, AlexNet  
60 [12] has been used as a pre-trained model to perform feature extraction from ECG profiles and predict  
61 for cardiac arrhythmia with 92.4% accuracy [14]. An ECG biometric recognition using convolutional  
62 neural networks (CNNs) has also been tested, attaining a similar error percentage of 2.26% [15] and  
63 93.6% precision in the screening of paroxysmal atrial fibrillation [16]. However, when kNN and  
64 support vector machine (SVM) models are attached on the top of the CNN feature, the precision  
65 drops to 90.7% and 92.9%, respectively. This shows that the traditional pipeline involving the  
66 selection of feature extraction and classifier modules is outperformed by an end-to-end trainable DL  
67 model.

68 A multimodality is preferable to a single modality in DL models, and can involve various  
69 biometric inputs such as ECG, facial images, fingerprints, voice, ear images, and iris data. Any model  
70 using single modality appears to be easily corrupted by powerline fluctuations, surrounding noises,  
71 electromyography (EMG), movement artifacts, and electrodes, so the challenge lies on developing  
72 accurate unimodal identification algorithms. Noise reduction techniques have been tested to  
73 overcome these effects [17], but multimodality has many additional benefits. If the signal-to-noise  
74 ratio of one modality is low, offsetting the effects can be performed by another to maintain the  
75 cumulative performance. Furthermore, latent correlations between modalities can be trained to  
76 improve the performance. Finally, it is easier to train multimodal models than multiple independent  
77 models for each modality.

78 An appropriate fusion method should also be combined with multimodal models, particularly  
79 a feature-level fusion, because it accommodates correlations between modalities. However, the  
80 algorithms before and after the feature-level fusion are performed independently, allowing any  
81 errors that occur before the fusion can accumulate. The end-to-end training of the system minimizes  
82 such accumulated errors.

83 Incomplete ECG profiles can be overcome by a multitask learning. In real-world settings, ECG  
84 data are influenced by factors such as heart rate and disease. Such factors can be marginalized if the  
85 model can be trained by the multitask learning to focus on the target task and ignore other factors.  
86 When implementing the multitask learning, the loss of each task can be weighted and a suitable  
87 method to determine weightings is therefore required. In this paper, our tasks are person  
88 identification and gender classification: if the former is well trained, then the latter would also show  
89 an improvement in performance. In other words, if the identification is difficult to train, then gender  
90 classification can help to train the network. The benefit of multitask learning is that deficiencies in  
91 one task helps to regularize the other, so that the training constructively progresses regardless of  
92 incompleteness of either characteristics of personal identification or gender classification.  
93 Accordingly, one model can perform two tasks by comparing the models trained on each task.

94 ECG in the wild could also contain noise because it may be collected from various devices  
95 differing in precision (e.g., smart watches, smart bands). It may also contain errors, or outliers, which  
96 could be due to faulty instruments, data transmission/interference or technology compatibility issues.  
97 The condition of the subject at the time of measurement also has an influence on noise. Similarly,  
98 facial image data can be affected by the viewing angle, brightness, and blurring, while fingerprint

99 data can be influenced by the position and pressure of the fingers. The model architecture must  
100 therefore be robust and must consider a generalization. Therefore, the proposed model is also  
101 relevant and applicable to intelligent home systems where the access is granted using **biometrics** of  
102 the household members. The main contributions of the work described in this article can be  
103 summarized as follows:

104

- 105 • multimodal biometrics using combined facial image, fingerprint, and ECG data,
- 106 • multitask learning for personal identification and gender classification tasks,
- 107 • feature fusion methods using a deep neural network,
- 108 • end-to-end trainable architecture, and
- 109 • a robust model under noisy and/or incomplete data situations.

110

111 The rest of the paper is structured in the following. Section II discusses related work on modality,  
112 fusion methods and multitask learning. Section III describes preprocessing, architecture, and deep  
113 learning methods for user identification and gender classification. Section IV discusses our  
114 experimental results under various conditions, and Section V concludes with the provision of follow-  
115 up research direction.

## 116 2. Related Work

### 117 2.1. ECG Analysis

118 ECG profiles provide useful biometric data because the electrical properties of the heart carry  
119 unique information suitable for personal identification or authentication [18–21]. Among various  
120 approaches that have been tested, single-lead ECG data collected across 19 subjects was fed into a  
121 Ziv-Merhav cross-parsing algorithm, which achieved 100% accuracy for a larger number of  
122 experiments [2]. Other successful methods include SVMs [3, 4], qualifying similarity or dissimilarity  
123 [5], and random forest models [6]. Personal identification has also been achieved by analyzing the  
124 frequency features of ECG signals without a fiducial point [7, 8] and classifying the shape of heart  
125 rate variability by principal component analysis and linear discriminate analysis [1, 9].

### 126 2.2. Multimodal Learning

127 Multimodal learning can combine multiple types of biometric data to recognize or authenticate  
128 users, and the fusion of multimodal features can increase the accuracy of verification [22, 23]. For  
129 example, combined ECG and fingerprint data achieves greater accuracy than either of the individual  
130 modes [24][25]. The uncertainty in the time domain features of ECG was 5.0% [18], but by combining  
131 ECG and facial image data this was reduced to 1.0% [23]. Finally, the accuracy of personal  
132 identification using palm prints (82.1%) or ECG (89%) was increased to 94.7% by combining them  
133 into a multimodal model [26]. **Recently, multimodal biometric identification system was presented**  
134 **using ECG and PPG [27].** In addition to multimodal learning research related to user identification  
135 using ECG, there are various multimodal learning studies related to disease diagnosis using magnetic  
136 resonance imaging (MRI) [28–30].

### 137 2.3. Handling Multimodal Databases

138 Multimodal databases are handled by constructing either a true or virtual database to combine  
139 the unimodal data. True multimodal databases provide all the biometric data from real people.  
140 However, this is an expensive and time-consuming process. There is a limited set of data that can be  
141 gathered, and the risk of losing personal information increases. Most studies in this area, therefore,  
142 use virtual multimodal databases, which are quicker and easier to assemble [31–35]. Given two  
143 mutually exclusive subject-based databases, a virtual multimodal database would be formed by  
144 pairing subjects in each database so that the data for each subject would be combined. Achieving this  
145 is possible by assuming that a single subject can independently be represented using a variety of

146 biometric traits [35]. Currently, there is a lack of accurate multimodal database in the public domain  
147 possessing face, fingerprint and ECG data.  
148

#### 149 *2.4. Feature Fusion Techniques*

150 As data propagates from the input layer to the label, fusion can be achieved at five different  
151 stages, namely the input, feature, score, decision and rank.

152 Input-level fusion means that the data are concatenated or fused and then used as the model  
153 input. This approach is suitable if each modality has the same data type. The input-level fusion is  
154 not widely used because most modalities have different data types, which need to be extracted in an  
155 independent manner.

156 A feature-level fusion integrates different features from multiple biometrics, thus, constructing  
157 a dataset by concatenating each independent biometric [36]. Little progress was made for a long time  
158 due to implementational challenges, but more recent work has been successful with the feature-level  
159 fusion in three different scenarios [37] as well as the feature-level concatenation of face and  
160 fingerprint data [38].

161 A score-level fusion achieves a good level of compromise between the simplicity of  
162 implementation and effectiveness given that it is more accessible than input-level or feature-level  
163 fusion but can nevertheless achieve successful matches with incomplete data. Many score-level fusion  
164 approaches have therefore been reported, including those using Bayesian framework [39] and  
165 density-based methods [40]. The effectiveness of score-level fusion reflects the presentation of results  
166 as raw scores, quantized scores, or probabilities when biometric traits are combined and features are  
167 matched. However, one disadvantage of the score-level fusion is given by the diversity of scores  
168 acquired from a variety of matching strategies.

169 A decision-level fusion generates a binary outcome (yes or no) as typically applied in a personal  
170 identification scenario (identified/present in database or not identified/not present). The decision-  
171 level fusion is therefore used for other binary outcomes such as majority voting [41] or Boolean  
172 operations [42]. Despite the simple and intuitive outcome, the decision-level fusion is less popular  
173 than the score-level and the rank-level fusions because certain types of data cannot be adapted to this  
174 strategy naturally.

175 Finally, a rank-level fusion consolidates larger than two results from identification to improve  
176 the reliability of a recognition task, and is therefore popular in the domains of data mining and  
177 pattern recognition. Variations of the rank-level fusion method include top rank [43], Borda count  
178 [44], weighted Borda count [45] as well as Bayes fuse based on a Bayesian inference [46, 47]. The  
179 performance of this strategy keeps improving, as shown in the mixed group ranks method [48].

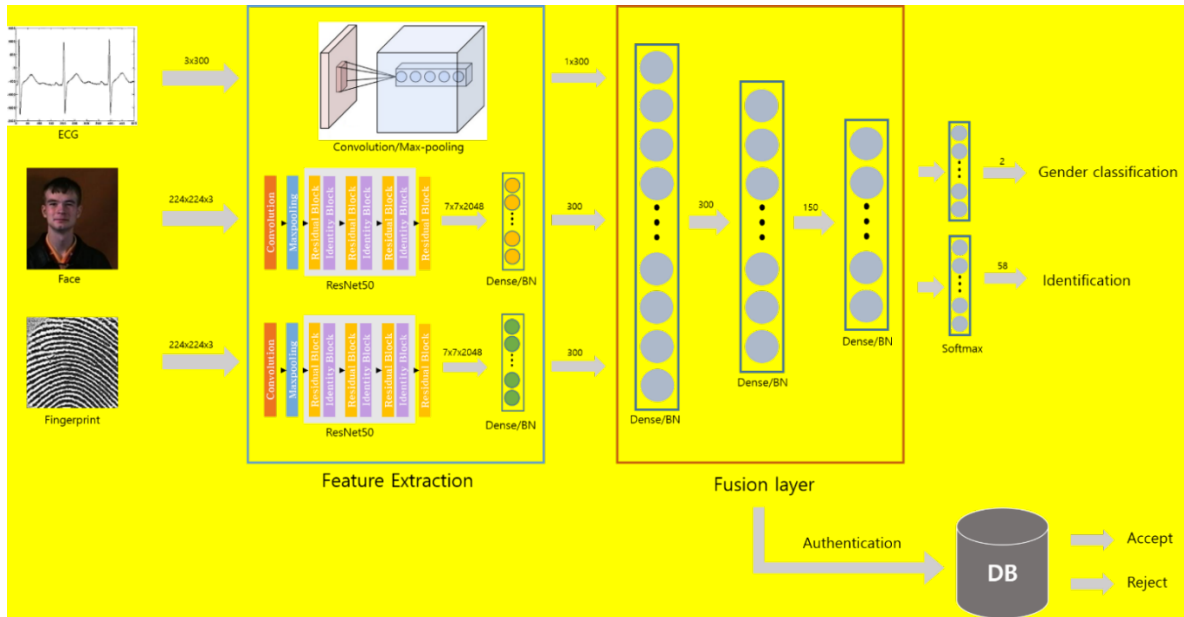
#### 180 *2.5. Multitask Learning*

181 A multitask learning intends to exploit meaningful information embedded in a variety of  
182 connected tasks to enhance generalization across all the relevant tasks. It can be utilized to identify  
183 several features at once, such as the recognition of gender, age and identity using an ensemble of  
184 features subjected to decision tree and Bayes network analysis [49]. The multitask learning allows the  
185 sharing of representations between tasks, and the execution of the main task can sometimes be  
186 enhanced by utilizing knowledge from other tasks [50]. In contrast to optimizing the learning of  
187 individual tasks, multitask learning considers a set of interrelated tasks that must be solved, and the  
188 performance is enhanced by jointly executing the tasks and exchange the data representing different  
189 features [51]. To reduce learning bias, multitask learning can be combined with other learning  
190 techniques such as semi- or unsupervised, reinforcement, active, multi-view, and graphical models.  
191 Many groups have applied multitask learning to ECG profiles, and a deep multitask learning model  
192 with additional network fine-tuning has increased the accuracy of the ECG signal evaluation by 5.1%  
193 [52].  
194  
195

196

197 **3. Methods**

198 Our network architecture is organized into three different components, namely a feature  
 199 extraction that converts the input into the embedding space, a fusion layer that integrates features,  
 200 as well as a task layer that carries out the operation (Fig. 1). The feature extraction is accomplished in a  
 201 unique manner on each modality, given their specific characteristics. The data for fingerprint ( $x_p$ ) and  
 202 face ( $x_f$ ) biometrics are static images, whereas the ECG data ( $x_e$ ) are temporal signal traces. Classifiers  
 203 trained on sizeable databases might be applied as an established feature extractor [53]. We employed  
 204 Residual Network 50 (ResNet50) to extract features using  $x_f$  and  $x_p$ .  
 205



206

207

**Figure 1.** Comprehensive network architecture of the multimodal deep multitask learning system.

208

209 A fully connected (FC) layer was considered to align the ECG data with the dimension number.  
 210 The CNN was continued by a max pooling component intended for  $x_e$  (ECG data) with the purpose  
 211 of removing reliance on a temporal axis for the extracted feature. The fusion layer (neural network)  
 212 considers chained features as the input from the feature extraction component. Following up the data  
 213 propagation, information representing every modality is combined to reduce the overall loss. It is  
 214 concluded by the task layer using the combined features from the fusion layer as its input, and  
 215 classification is performed after a single layer, with the node quantity specifying the class quantity.

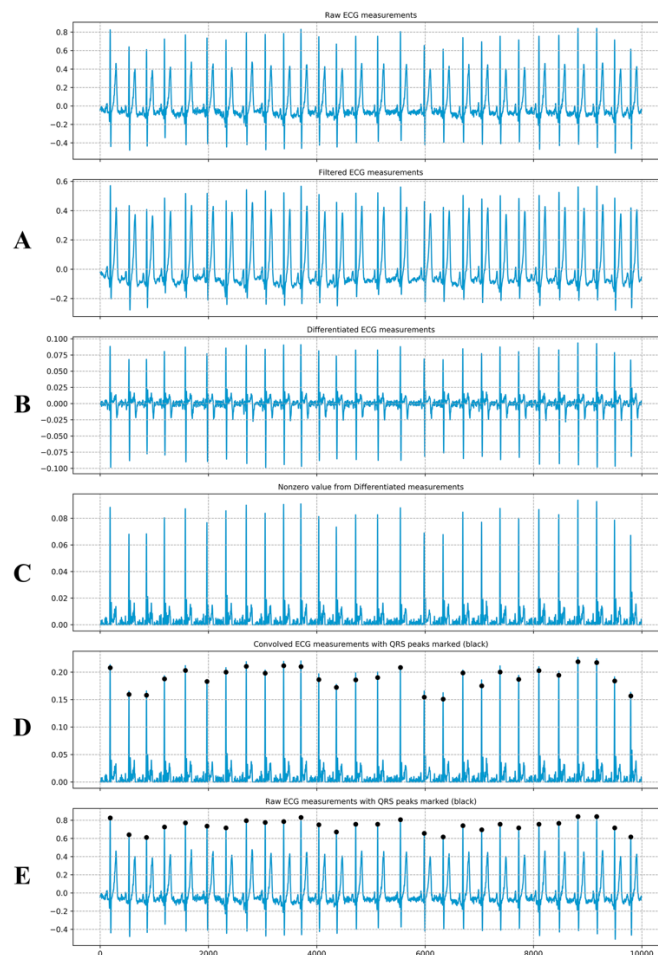
216 **3.1. Preprocessing**217 **3.1.1. Face and Fingerprint Data**

218 As stated above, only limited data are available for user identification in multimodal datasets,  
 219 thus, more facial images and fingerprints are required to implement a generalized network. The  
 220 augmentation of facial images and fingerprint data was achieved by rotation, translation and  
 221 cropping (the latter not for facial images, because the entire face is needed for identification). Images  
 222 were rotated from  $-30^\circ$  to  $30^\circ$  in  $5^\circ$  intervals to obtain 12 new images per original image. For  
 223 translation, each image was translated from  $-5$  to  $5$  pixels in 1-pixel intervals to obtain 10 new images  
 224 per original image. For cropping, we created images with 60% of the original size at random positions  
 225 in the original image to obtain 47–50 new images per original image. After augmentation, we used a  
 226 transfer-learning technique where a pre-trained neural network, ResNet50 is adopted to extract  
 227 features comprising a set pair of fingerprint and facial images.

## 228 3.1.2. ECG Data

229 The Pan Tompkins QRS detection algorithm is well-known to find the R peak, which is the center  
 230 of the QRS complex within the ECG signal. Herein, the ECG signal is passed through low and high  
 231 bandpass filters, and differential values are obtained for peak detection based on these data. During  
 232 this process, we determine the threshold ECG peak value and the minimum time to generate the R  
 233 peak, yielding candidate groups for actual R peaks. The detection algorithm calculates the differential  
 234 values and then squares each value for detecting the peak. Values are set to zero if the peak is  
 235 negative, as it is not intuitive to retain them.

236 The R peak detection process was implemented as shown in Fig. 2. Initially, a bandpass filter is  
 237 considered to sharpen the peaks and smooth the rest of the signal. The original value is then  
 238 subtracted from the present value in the filtered signal to calculate the differentiated signal. Following  
 239 the replacement of any negative values with zero, the peaks are derived from candidate points that  
 240 are greater than both the previous value and the next value. Finally, to validate the computed R peaks,  
 241 the algorithm superimposes the peak indices with the same indices in the original ECG signal. If the  
 242 overlaps are confirmed, the indices are stored. Having applied the Pan Tompkins QRS detection  
 243 algorithm, we added one more step to account for any delay compared to the raw signal. The  
 244 additional step ensures that, if there is a peak value larger than the detected peak value in the adjacent  
 245 range, we set the larger peak value as the R peak value.  
 246



247 **Figure 2.** Process for R peak detection. (A) Application of a bandpass filter, (B) differentiation, (C) clipping  
 248 of negative values to zero, (D) detection of maximum points, and (E) matching to the original signal.  
 249  
 250

We processed a quantity of 300 data samples prior and post R peak detection to produce a vector representing the QRS complex. Following this mechanism, we normalize each QRS complex using a min-max method.

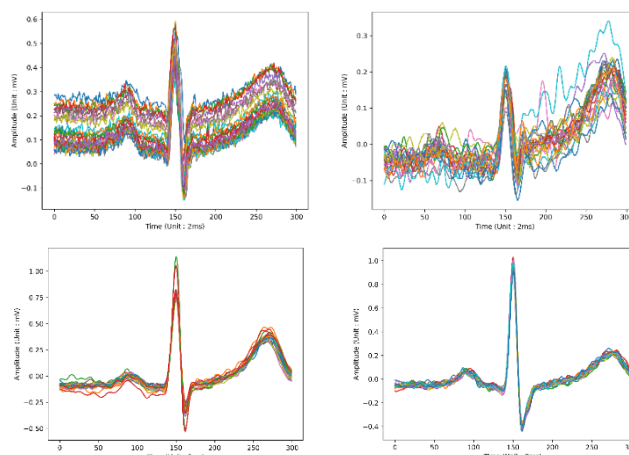


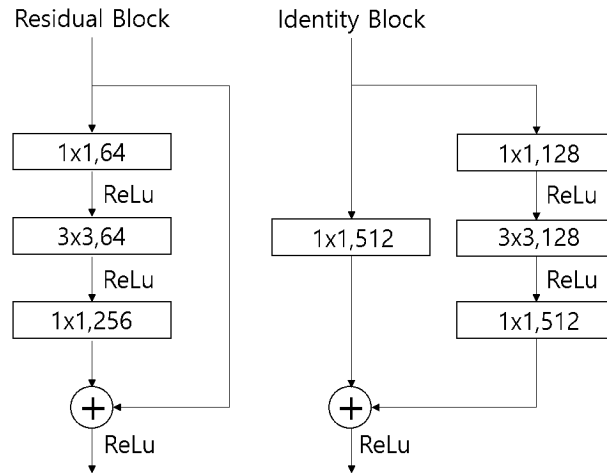
**Figure 3.** Four examples of QRS compositions extracted from the same record. The compositions on the top row show consistency within the record, but those on the bottom row show irregularities within the record.

Given the less importance nature of the inter-QRS complexes temporal information, compared to the complexes themselves, we extracted three QRS complexes to make one input. A single sequence therefore possesses three time-steps, indicating formation of this sequence using a group of three QRS complexes. The extracted QRS complex, based on the R peak in each recording and plotted in the same grid, is captured in Fig. 3. The consistency of the R peak wave varies depending on the records.

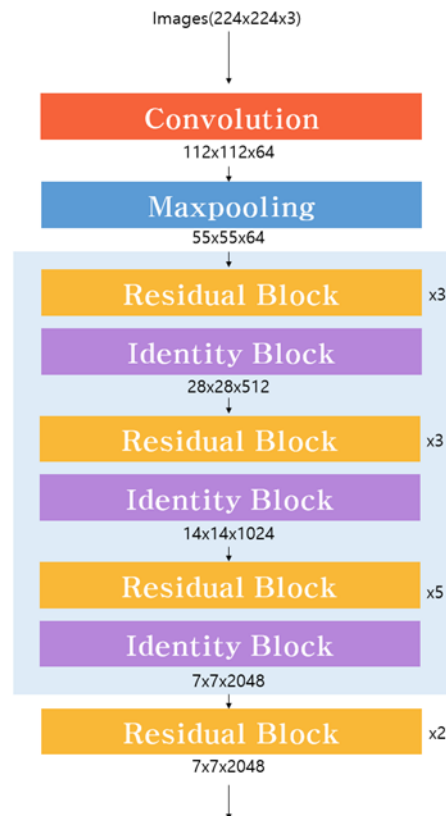
### 3.2. Feature Extraction

#### 3.2.1. ResNet50

ResNet is a known method to perform feature extraction from image data [54]. It has been constructed via training of ImageNet, one of the comprehensive datasets for object classification. Herein our feature extraction method used ResNet50 that is applied to our face/fingerprint images, with mean pooling of features ( $7 \times 7 \times 2048$ ). The input size of the images was set to  $224 \times 224$ . ResNet50 is a CNN with 50 layers that is trained to classify images into 1000 categories in the ImageNet database. It comprises a convolution layer ( $3 \times 3$  filter), a max-pooling layer and a residual network comprising a residual block and identity block as depicted in Fig. 4. The overall structure is given in Fig. 5. The output shape after the identity block is described at the bottom of each identity block box in Fig. 5.



277  
278 **Figure 4.** Detailed structure of the residual and identity blocks. The residual block allows direct connection  
279 from input to output, whereas the identity block uses an identity matrix instead of a direct connection.  
280



281  
282 **Figure 5.** The architecture of ResNet, comprising a convolution and a max-pooling layers, followed by series  
283 of alternating residual and identity blocks.

### 284 3.2.2. CNN Model for ECG

285 Although models based on long short-term memory architecture has been widely applied for  
286 identifying [55], the CNN was employed herein to extract features, seeing the less importance nature  
287 of inter-QRS temporal information, in comparison to the actual complexes. For the CNN, we have a  
288 one-dimensional convolution layer, which considers a tensor with shape (batch size, time step, 300)  
289 as an input and yields an output tensor with a similar shape characteristics. This is then followed by  
290 operating a single max-pooling task. The results of ECG feature extraction are chained with two  
291 feature vectors arising from the different modalities (Fig. 6).

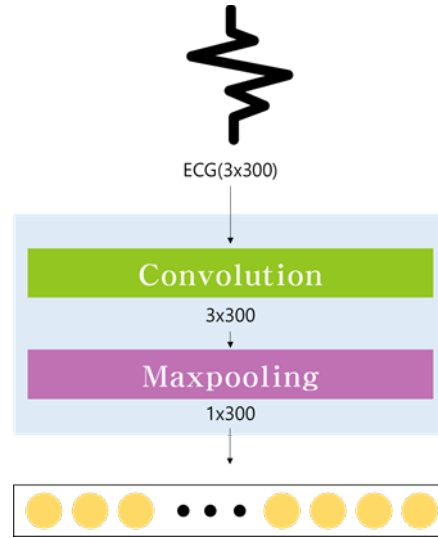


**Figure 6.** The one-dimensional CNN used to extract ECG features.

292  
293

### 294 3.3. Feature Fusion

295 Input level fusion using three different modalities effectively is difficult. We thus compared the  
296 score-level fusion with feature-level fusion. For fusing at the score level, we tested three techniques,  
297 namely sum, product and max rule. In the case of fusing the features, three features were extracted  
298 from every modality for normalization as well as concatenation as the model inputs.

### 299 3.4. Classification

300 Our proposed system has to decide the most likely class for each test case. We therefore used the  
301 softmax activation function, which considers the class-wise outputs and their transformation into  
302 corresponding probabilities via Eq. (1):  
303

$$\text{Softmax}(y_i) = \frac{\exp(y_i)}{\sum_j \exp(y_j)} \quad (1)$$

304  
305  
306  
307  
308  
309  
310

Herein  $y$  denotes the network output with the same dimension as the class count, and  $y_i$  is the  $i^{\text{th}}$  component of  $y$ . Note that Eq. (1) ensures that normalization of the exponential numerator by the sum of exponential terms in the denominator. The class with highest number is the target class. For identifying users and classifying genders, the cost function considered the cross-entropy loss during the model training. The function can be computed using Eq. (2):

$$H(y, \hat{y}) = - \sum_i y_i \log(\hat{y}_i) \quad (2)$$

311  
312  
313  
314  
315  
316

Here we have  $y$  and  $\hat{y}$  denoting the output and original distributions, respectively. The logarithm usage in Eq. (2) corresponds to penalty being applied for incorrect predictions, i.e., high loss with divergence of the predicted class from the real label. Eq. (2) does not represent a symmetrical function with  $H(y, \hat{y}) \neq H(\hat{y}, y)$  because only the logarithm of predicted probabilities is considered.

### 317 3.5. Joint Loss

318 Joint training of the network to simultaneously handle more than one tasks was performed by  
319 applying a joint loss that integrates cross-entropy (binary) for classifying genders ( $L_1$ ) and cross-  
320 entropy (categorical) for identifying users ( $L_2$ ). Two losses were weighted and summed for final loss

321 calculation in the model training. The formula for each loss is shown in Eq. (3)-(5). The most favorable  
 322 indicators for  $w_1$  and  $w_2$  in Eq. (5), where the sum is 1, were found experimentally.  
 323

$$L_1 = -y \log \hat{y} - (1 - y) \log(1 - \hat{y}) \quad (3)$$

$$L_2 = - \sum_i y_i \log \hat{y} \quad (4)$$

$$L_{joint} = w_1 \times L_1 + w_2 \times L_2 \quad (5)$$

### 324 3.6. Optimization

325 For optimizing parameters, Adam, an efficient procedure for the gradient-based optimization of  
 326 stochastic objective functions, was utilized relying on lower-order moments adaptive estimation [56].  
 327 This takes advantages of the two well-known methods, namely AdaGrad and RMSProp [57, 58].  
 328 Parameter optimization was achieved as shown in Eq. (6) and (7).  
 329

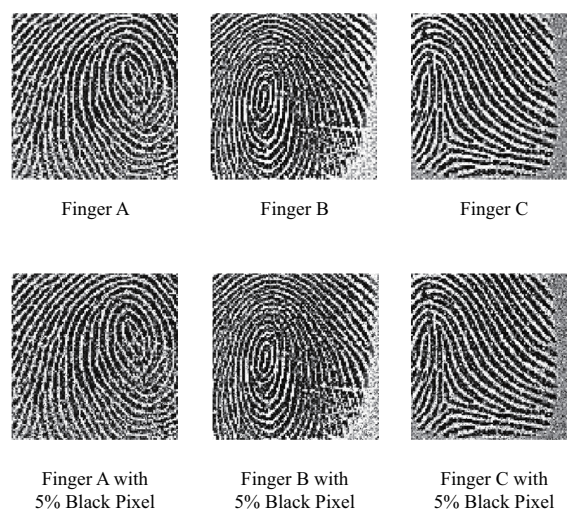
$$\alpha_t = \alpha \cdot \sqrt{1 - \beta_2^t / (1 - \beta_1^t)} \quad (6)$$

$$\theta_t \leftarrow \theta_{t-1} - \alpha_t \cdot m_t / (\sqrt{v_t} + \epsilon) \quad (7)$$

330 where  $\alpha_t$  is the step size at time-step  $t$  and  $\beta_1, \beta_2$  are rates characterizing exponential decrement  
 331 for moment estimation. To calculate the updated parameter vector  $\theta_t$ , we used updated biased  
 332 moment estimates ( $m_t, v_t$ ) and  $\alpha_t$ .  
 333

## 334 4. Experiments

335 Nine experiments were conducted to investigate the behavior of the new model. The first  
 336 experiment considered multitask learning (identifying users and classifying genders) using single  
 337 modality and multimodality. The second experiment compared multitask and single-task learning  
 338 based on multimodal biometrics comprising ECG data from ECG-ID [59, 60], PTB [59, 61]), facial  
 339 images (Face95 [62]) and fingerprints (FVC2005 [63]). The third experiment tested the user  
 340 authentication using two distance metrics. The fourth experiment added noises to the data to verify  
 341 the robustness of the model.



342  
 343 **Figure 7.** Noise in the fingerprint input data for the multimodal deep multitask learning system.

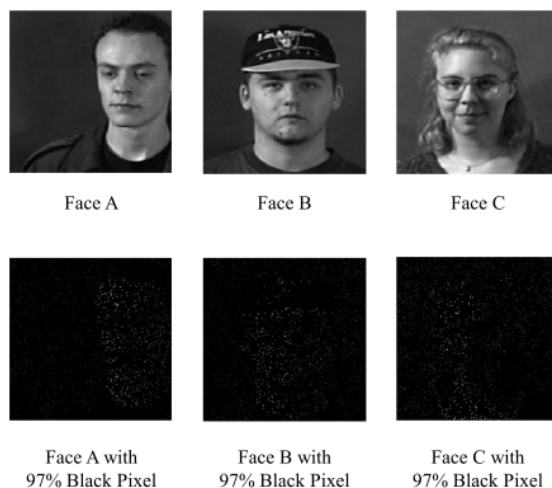


**Figure 8.** Noise in the face input data for the multimodal deep multitask learning system.

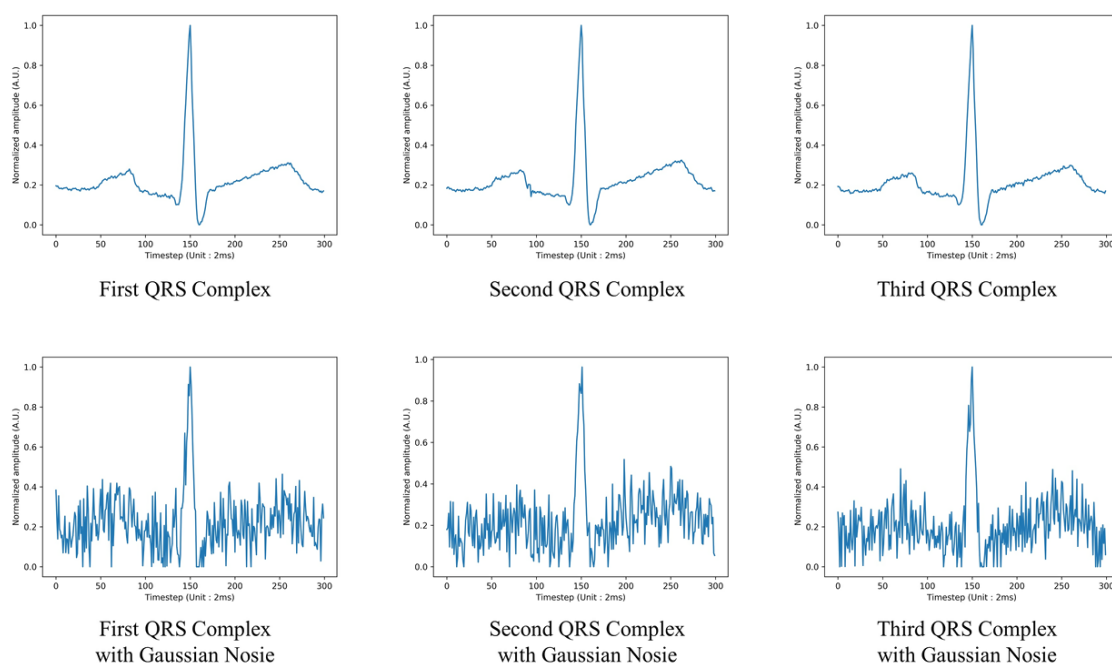


**Figure 9.** Noise in the ECG input data for the multimodal deep multitask learning system.

The fifth experiment investigated the impact on performance when one or two of the three biometric datasets were missing. The sixth experiment compared the performances of feature-level and score-level fusions where the latter based on sum, max or product rules. The seventh experiment modified the joint loss to give various weights. The eighth experiment investigated how data augmentation affected the performance of the multimodal/multitasking model. The final experiment changed the hyper-parameters of the fusion model to find the optimal architecture. The number of nodes was changed to compare the accuracy of each task (user identification and gender classification).

#### 4.1. Dataset

##### 4.1.1. ECG Data

The ECG-ID has 310 records from 90 subjects with composition: 44 males and 46 females with ages from 13–75 years. Each single-lead trace was observed and stored for 20 s and sampled at 500

361 Hz at 12-bit resolution. The range of observation is  $\pm 10$  mV. The dataset provides not only raw signals  
362 (EC I), but also processed signals with high-frequency and low-frequency noises filtered out (ECG I  
363 filtered). Associated data include subject age, gender and recording date.

364 The PTB ECG has 549 records from 290 subjects with composition: 209 males and 81 females  
365 with ages from 17–87 years. Every record comprises 15 concurrently measured signals, namely the  
366 standard 12 leads (i, ii, iii, avr, avl, avf, v1, v2, v3, v4, v5, v6) along with the three Frank lead ECGs  
367 (vx, vy, vz). Every signal is sampled at 1 kHz and at 16-bit resolution. The range of observation is  
368  $\pm 16.384$  mV. Associated data include a comprehensive clinical summary, gender, age and diagnostic  
369 classes. To ensure an identical sampling rate to ECG-ID, PTB ECG signals were resampled at 500 Hz.

#### 370 4.1.2. Facial Images

371 The Faces95 database contains 1440 images with composition: 72 male and female subjects (20  
372 per subject), primarily bachelor-level students. The images are portrait formatted and have resolution  
373 of  $180 \times 200$  pixels. For data gathering purposes, the subjects take a single step movement  
374 approaching the camera to simulate realistic changes such as variations in head scale and lighting as  
375 well as face position translation. The images also show variations in facial expression, but no variation  
376 in hair style.

#### 377 4.1.3. Fingerprint Images

378 The FVC2006 database has 7200 images from 150 subjects, each image based on four sensors  
379 (1800 images per sensor) with different resolutions: electric field sensor ( $96 \times 96$  pixels), optical sensor  
380 ( $400 \times 560$  pixels), thermal sweeping sensor ( $400 \times 500$  pixels) and SFinGe v3.0 ( $288 \times 384$  pixels). The  
381 dataset is segmented into subsets. Each of the subsets DB1-A to DB4-A has 140 subjects with 12  
382 images per subject, giving 1680 images per subset. Each of the subsets DB1-B to DB4-B has 10 subjects  
383 with 12 images per subject, giving 120 images per subset.

#### 384 4.1.4. Virtual Dataset

385 A total of 58 virtual subjects were produced to decrease the variability. Because the subjects in  
386 the Face95 database are primarily bachelor-level students, it was viewed that the ages of the virtual  
387 individuals ranged from teens to thirties. The gender information was labeled by two different  
388 annotators in a complete affirmation. Utilizing criteria from the labeled gender and the age range, a  
389 valid sample was selected, matching age/sex variables from the ECG dataset with the face attributes.  
390 To ensure accuracy and fairness, we selected the scanner type used when the subjects were  
391 fingerprinted by using the fingerprint images in subset DB1-A of the FVC2006, and arranged each  
392 image randomly with the virtual subject already assigned to ECG and face data. Virtual subjects were  
393 therefore designed with three modalities (face, fingerprint and ECG) according to the gender and age  
394 labeled in the dataset.

### 395 4.2. Results

#### 396 4.2.1. Comparison of the Unimodal and Multimodal Models

397 Like earlier models, the proposed model achieved the perfect accuracy based on the individual  
398 modalities of the ECG-ID, Face95 and FVC2006 datasets. There is no possibility to compare the  
399 performance of different models if the accuracy in a test scenario is 100%, so we added noise to  
400 achieve better generalization and discrimination (Figs 7–9). To the ECG dataset, we added Gaussian  
401 noise whose standard deviation is 0.1 for a series of three normalized QRS complexes. For the  
402 fingerprint images, we selected 5% of the pixels and changed the color to black. And for the facial  
403 images, we selected 97% of the pixels and changed the color to black.

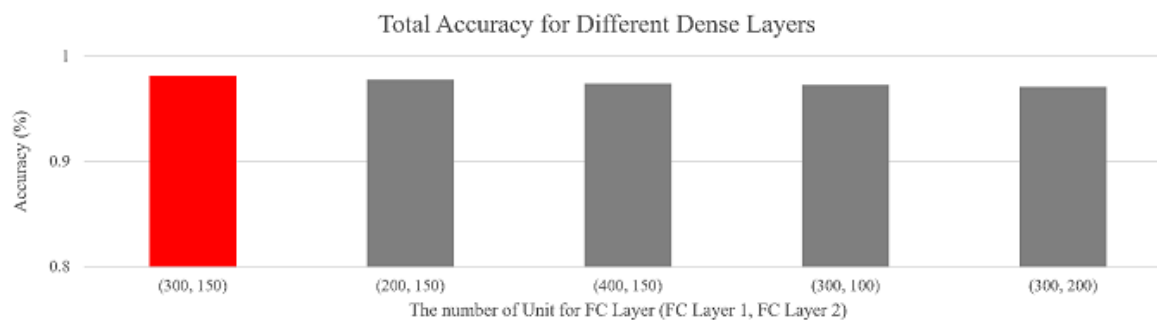
404 The new model takes account of multimodality by propagating each modality to a feature  
405 extraction module, where it is represented by the fixed size of embedding (the same size for each  
406 modality). Unimodal and multimodal models were distinguished in terms of performance by the

407 specific inclusion or exclusion of modalities. Changing the number of input modalities also changed  
 408 the output of the feature extraction module. Based on the extracted feature embedding, user  
 409 identification and gender classification are therefore carried on in the fusion and classification layers.  
 410 The results of the unimodal and multimodal experiments are compared in Table 1.

411 Each experiment was carried out three times with different random seeds for initializing  
 412 associated weights, and the average results in each case were reported to avoid biases caused by the  
 413 parameter initialization. For the identification of virtual subjects, the accuracy was  $\leq 85\%$  when using  
 414 a single modality, but this increased to  $>90\%$  when using two or three modalities, with the highest  
 415 score achieved when all three modalities were included (98.28%).

416 Similarly, the multimodal models achieved better gender classification results ( $>93\%$  accuracy)  
 417 than models based on a single modality, and the model combining all three modalities showed the  
 418 highest performance (97.70%).

419 These results using a feature-level fusion confirm that the user identification works well even if  
 420 there are noises in the input biometric data and that three modalities provide more accurate results  
 421 than two. The suitability of deep and wide networks for the merging of three modalities is unclear,  
 422 so the use of hyper-parameters in the fusion layer should be explored. Fig. 10 demonstrates the  
 423 consequences of changing the node quantity in each FC layer when processing noisy data from a  
 424 virtual database. We did not add further layers because this increases the computational  
 425 requirements and the size of the model.



426  
 427 **Figure 10.** The total accuracy of user identification and gender classification depending on the number of nodes  
 428 in each fully-connected (FC) layer.

429  
 430

**Table 1.** Multitasking accuracy for different combinations of modalities (feature-level fusion).

Modality			Task		Accuracy (%)	
ECG	Face	Finger	ID	Gender	ID	Gender
✓			✓		77.49	-
✓				✓	-	91.95
	✓		✓		76.44	-
	✓			✓	-	88.51
		✓	✓		83.91	-
		✓		✓	-	90.80
✓	✓		✓		95.98	-
✓	✓			✓	-	93.68
✓		✓	✓		94.83	-
✓		✓		✓	-	95.40
	✓	✓	✓		96.55	-
	✓	✓		✓	-	94.83
✓	✓	✓	✓		98.28	-
✓	✓	✓		✓	-	97.70

431

432

**Table 2.** Comparative performance of single- and multi-task learning models.

Task		Accuracy (%)	
ID	Gender	ID	Gender
✓		98.28	-
	✓	-	97.70
✓	✓	98.97	96.55

433

434

435

436

437

438

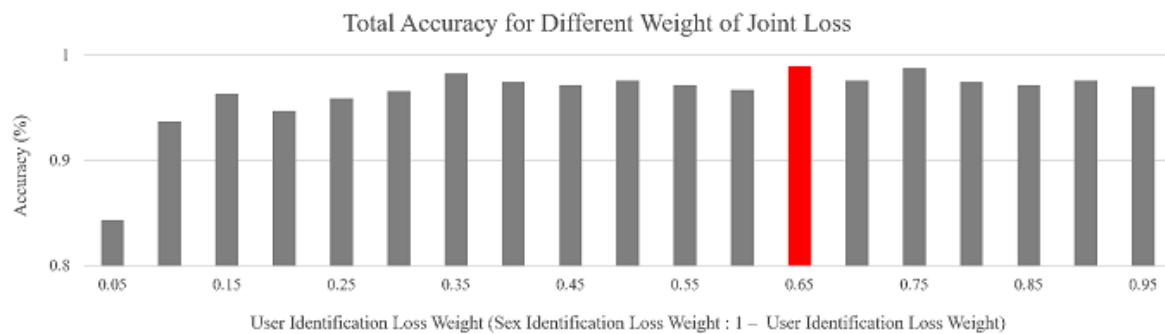
439

440

441

442

The number of nodes in each FC layer was initialized as 150 for the first and second layers, resulting in 900 features after feature fusion. We obtained at least 600 features from two of the three biometric datasets (ECG, facial image and fingerprint). Fig. 10 also summarizes the performance achieved in the experiment and demonstrates the benefits of FC layers with (300,150) nodes, which increased the accuracy of user identification and gender classification to 98%. Our model also outperformed the baseline approach with 300 nodes in the first FC layer and 200 nodes in the second (the poorest performance in this experiment). We therefore found that the (300,150) approach achieved the greatest accuracy in this experiment on the virtual database, and confirmed that the performance of the model degrades if the number of nodes is too large or too small.



443

444

445

**Figure 11.** The total accuracy of user identification and gender classification using different sets of joint loss weights.

446

#### 4.2.2. Single- and Multi-Task Learning

447

448

449

450

451

452

453

454

455

456

457

458

459

460

461

462

463

464

465

466

Single- and multi-task learning were compared by adding a loss term as necessary in each experiment. For example, when a gender classification was omitted, the loss function only contained the log likelihood of user-identity classification. However, in multitask learning experiments we included the cross-entropy of user identification and gender classification, and the balance between the two loss functions was controlled by the joint loss weight. The optimized weights were determined experimentally as follows. The performance of the multimodal and multitask model was evaluated on the virtual database with noises. The joint loss weight was varied from 0 to 1 in increments of 0.05. The parameters of the network were initialized according to different random seeds for each experiment. Also, six runs were carried out and averaged to reduce the bias. The final joint loss weights were 0.65 and 0.35 for identifying users and classifying genders, respectively. The performance of our model surpassed that of the baseline approach that applies uniform weights (0.5) for both tasks, and the improvement was greatest for the user identification task (Fig. 11). This confirmed that each task shared features with different weights to enhance the performance of multi-task in comparison to a single-task learning. As shown in Table 2, the multitask learning achieved 0.69% better score in the user identification task but the single-task model was 1.15% better for gender classification. This reflects the trade-off relationship inherent in multiple tasks. For example, adding loss weight to the identification task achieves a better performance in this task, but reduces the accuracy of gender classification. For this context, we took the mean of the identification and classification tasks as the model performance. Even if we are unable to achieve the greatest accuracy for gender classification, it excels the user identification accuracy. We can also see the improve

467 efficiency in our proposed multi-task model due to equal predictive performance at a half training  
 468 time, in comparison to the single-task counterpart.

469

470

**Table 3.** Confusion matrix obtained during authentication.

Data Type		Threshold	FAR (%)	Accuracy (%)
Non-Augmented	Euclidean	6.02–8.56	0.0	100
	Cosine	0.14–0.32	0.0	100
Augmented	Euclidean	9.09	0.66	99.67
	Cosine	0.20–0.25	0.0	100

471

#### 472 4.2.3. Authentication

473 The authentication experiment incorporated a feature vector that consolidates three different  
 474 modalities (ECG, facial image and fingerprint) from the fusion layer. There is a trade-off during  
 475 authentication when the model inputs are unimodal data. For example, facial image data are easy to  
 476 obtain but their accuracy may be compromised by factors such as aging. Fingerprint data are highly  
 477 accurate, but the quality of the source material deteriorates over time. In a previous study [64], the  
 478 equal error rate of authentication was range of 2.69 to 3.07% using fingerprint data alone. We  
 479 conducted authentication experiments using multimodal data to overcome the tradeoffs inherent to  
 480 unimodal data and thus improve the performance.

481 We evaluated the authentication performance using our virtual dataset of 58 subjects. We  
 482 divided the subjects into two groups of 53 and 5, respectively, then picked 5 random subjects from  
 483 the group of 53 and combined them with the first group of 5. The authentication experiment therefore  
 484 involved 53 subjects in the database and 10 test subjects, allowing us to compare the similarity  
 485 between the two sets. The 53 subjects in the database also have feature vectors with average pooling.  
 486 Because each subject has nine features, the average pooling can represent the general characteristics  
 487 of the subject. In addition, we tested authentication with augmented data to prevent over-fitting and  
 488 to establish the general performance.

489 Similarity can be measured using various metrics, including the Euclidean distance that  
 490 represents the actual distance between two points and the cosine distance which is useful when the  
 491 vector size is not significant. With non-augmented data, the accuracy was 100% and the false  
 492 acceptance rate (FAR) was 0% when we applied an optimal Euclidean distance threshold range of  
 493 6.02 to 8.56 and optimal cosine distance threshold range of 0.14 to 0.32 (Table 3). With augmented  
 494 data, the accuracy was 99.67% with the Euclidean distance metric but 100% with the cosine distance  
 495 metric (Table 3). The authentication performance of the multimodal model is therefore near 100%.  
 496 The receiver operating characteristics (ROCs) for the non-augmented and augmented data are shown  
 497 in Fig. 12 and Fig. 13, respectively.

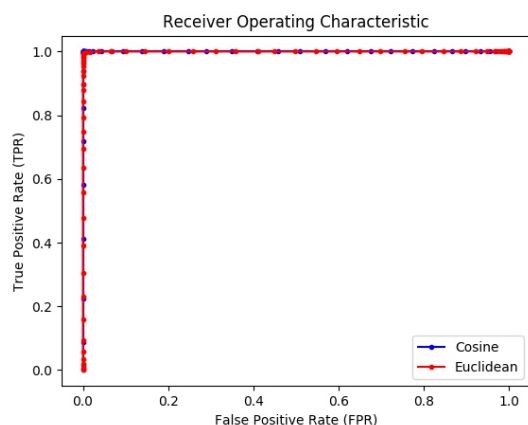


**Figure 12.** Receiver operating characteristics using non-augmented data.

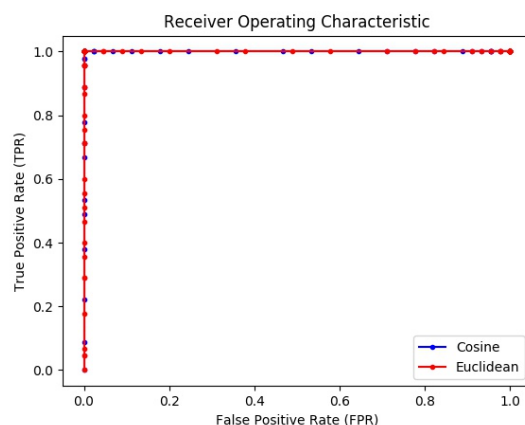


**Figure 13.** Receiver operating characteristics using augmented data.

498

#### 499 4.2.4. Robustness to Noisy Data

500 To determine whether our model is robust when presented with noisy data, we added noises to  
 501 one or more of the modalities during the user identification and gender classification tasks (Table 4).  
 502 For the identification task, the highest accuracy achieved with a single modality was 84.29% (for the  
 503 noisy fingerprint data). When the noises were added to two of the modalities, the highest accuracy  
 504 was 95.21%. However, when the noise was added to all three modalities, the accuracy increased to  
 505 98.97%. For the gender classification task, the best-performing single modality was ECG, with an  
 506 accuracy of 90.04% despite the noisy data. When the noise was added to two modalities, the highest  
 507 accuracy was 95.21% (noisy ECG and fingerprint data). When the noise was added to all three  
 508 modalities, the accuracy reached 96.55%. The observations herein confirm that the multimodal model  
 509 performs superior to models with any single modality when noises are included in the data. This  
 510 mirrors the results with clean data for user identification, where the best single modality (facial  
 511 images) achieved an accuracy of 99.42% but the trimodal approach achieved an accuracy of 100%. In  
 512 contrast, in the clean data experiment for gender classification, the trimodal approach achieved an  
 513 accuracy of 99.43% but was outperformed by the unimodal and bimodal models (100%). Overall,  
 514 these experiments demonstrate that that the trimodal model is robust to data, with only a 1.03% drop  
 515 in performance compared to the clean data for the user identification task.

516

517

**Table 4.** Unimodal and multimodal test for noise input.

Modality			Noise	Accuracy (%)	
ECG	Face	Finger		ID	Gender
✓			✓	80.08	90.04
	✓		✓	72.99	87.74
		✓	✓	84.29	88.70
✓	✓		✓	94.83	95.02
✓		✓	✓	93.68	95.21
	✓	✓	✓	95.21	92.91
✓	✓	✓	✓	<b>98.97</b>	<b>96.55</b>
✓				98.27	98.85
	✓			99.43	<b>100.00</b>
		✓		76.44	89.66
✓	✓			<b>100.00</b>	<b>100.00</b>
✓		✓		98.85	96.55
	✓	✓		<b>100.00</b>	98.85

✓	✓	✓	<b>100.00</b>	99.43
---	---	---	---------------	-------

518

519

**Table 5.** Accuracy of the multimodal model with incomplete biometrics.

Modality				Accuracy (%)	
ECG	Face	Finger	Noise	ID	Gender
✓			✓	31.61	82.18
	✓		✓	39.66	79.89
		✓	✓	52.30	83.91
✓	✓		✓	81.61	86.21
✓		✓	✓	<b>87.36</b>	<b>89.66</b>
	✓	✓	✓	<b>87.36</b>	89.08
✓				21.26	83.33
	✓			94.25	95.98
		✓		43.10	80.46
✓	✓			98.28	<b>98.28</b>
✓		✓		70.69	85.63
	✓	✓		<b>100.00</b>	97.70

#### 520 4.2.5. Robustness to Partial Modalities

521 In the experiments described above, the combination of modalities in the training and testing  
522 sessions were the same. However, in real-world there may be scenarios in which one or more of the  
523 modalities would be incomplete. To prove the robustness of the multimodal model when presented  
524 with incomplete input data, we trained the model using all three modalities but evaluated its  
525 performance with one or more missing, in the presence and absence of the noise (Table 5).

526 In the presence of artificial noise, the accuracy of the model never reached 90% regardless of  
527 which modality or modalities were omitted, but there was a jump in performance when the number  
528 of modalities increased from one to two, with all combinations of two modalities achieving an  
529 accuracy of 80% or more for both tasks. In the absence of artificial noise, the accuracy reached 100%  
530 for user identification and 98.28% for gender classification even in the absence of ECG data. The  
531 model therefore works well with limited biometric input if the noise in each dataset is weaker than  
532 the levels indicated in Fig. 7–9. Alternative models are not required as long as we can use at least two  
533 modalities.

#### 534 4.2.6. Fusion Techniques

535 Our new model uses fusion techniques to concatenate biometric characteristics, thus reducing  
536 the independent characteristics of each modality for reliability improvement and accuracy  
537 maintenance [65]. We compared feature-level fusion; which was applied prior to matching to  
538 aggregate the features into a single vector, and score-level fusion; which was applied post matching  
539 to compute the similarity level utilizing particular procedures (i.e., sum, product and max in our  
540 experiments) for every output to generate the final output vector (Table 6).

541 When using the feature-level fusion, the accuracy of user identification was 98.97% and the  
542 accuracy of gender classification was 96.55%. When using the score-level fusion, we found that the  
543 sum rule yields the accuracy of 98.85% and 99.42% for the same tasks. This represents an  
544 improvement of 2.87% for the gender classification, reflecting the robustness of the sum rule when  
545 exposed to noisy data [66]. For the score-level fusion method, the change of weights was also  
546 experimented for each modality, assigning a weight of 0.5 to one modality and 0.25 to the others. The  
547 results indicate that achieving the greatest accuracy is noted when the ECG weight is larger than or  
548 equal to the other modalities. Herein ECG appears to make the most significant contribution among  
549 the three modalities to improve the performance.

550

551

**Table 6.** Comparison of feature-level and score-level fusion methods.

Fusion Level	Rule	Weight			Accuracy (%)	
		ECG	Face	Finger	ID	Gender
Feature	-	-	-	-	<b>98.97</b>	96.55
		0.33	0.33	0.33	98.27	<b>99.42</b>
		0.50	0.25	0.25	98.85	<b>99.42</b>
		0.25	0.25	0.50	97.70	<b>99.42</b>
Score	Sum	0.33	0.33	0.33	96.55	89.08
		0.50	0.25	0.25	95.98	89.66
		0.25	0.50	0.25	93.10	89.08
		0.25	0.25	0.50	93.68	87.36
	Product	0.33	0.33	0.33	89.66	89.66
		0.50	0.25	0.25	89.66	87.93
		0.25	0.50	0.25	89.66	86.21
		0.25	0.25	0.50	89.66	87.36
Max	0.33	0.33	0.33	89.66	89.66	
	0.50	0.25	0.25	89.66	87.93	
	0.25	0.50	0.25	89.66	86.21	
	0.25	0.25	0.50	89.66	87.36	

## 552 4.2.7. Data Augmentation

553 A data augmentation virtually increases the amount of samples in the dataset using the existing  
554 ones while playing a role of a regularizer preventing the overfitting. It is particularly helpful for  
555 improving the performance in imbalanced class problems. We applied the data augmentation  
556 techniques described in preprocessing section and generated 455 data points for each modality. The  
557 experiments dealing with two tasks simultaneously were performed for each combination of  
558 modalities, but only the database was different. We found that the difference in the performance of  
559 the model when tested on the original and augmented databases ranged from 1.9% to 24.47%  
560 depending on the individual modality. When multiple modalities were used in the augmented  
561 dataset, the accuracy was always 99% or more. We therefore confirmed that data augmentation  
562 makes the model get generality, and that it is possible to create a model that attains high accuracy  
563 even with a small amount of data in real-world settings.

564

565

**Table 7.** Model performance with and without data augmentation.

Modality			Augment	Accuracy (%)	
ECG	Face	Finger		ID	Gender
✓				80.08	90.04
	✓			72.99	87.74
		✓		84.29	88.70
✓	✓			94.83	95.02
✓		✓		93.68	95.21
	✓	✓		95.21	92.91
✓	✓	✓		<b>98.97</b>	<b>96.55</b>
✓			✓	99.92	<b>100.00</b>
	✓		✓	97.46	98.31
		✓	✓	86.19	95.23
✓	✓		✓	<b>100.00</b>	<b>100.00</b>
✓		✓	✓	99.98	<b>100.00</b>
	✓	✓	✓	99.49	99.03
✓	✓	✓	✓	<b>100.00</b>	<b>100.00</b>

566

## 567 5. Conclusion

568 We have introduced a new multimodal and multitask learning model that uses ECG, facial  
 569 image and fingerprint features for user identification and gender classification. We have conducted  
 570 a number of experiments in an environment that assumes extreme noises, indicating that our model  
 571 is robust to noises, and have achieved greater accuracies than unimodal approaches. The proposed  
 572 model has also proven to be robust against the spoof attack problem that unimodal model is  
 573 vulnerable to. Our results show the desirable characteristics of our proposal. For identifying users,  
 574 classifying genders and authentication, our model outperforms other approaches reported in the  
 575 existing literature. The feature-level fusion ensures that the proposed model achieves similar  
 576 performances (over 80%) despite incomplete data (losing one out of the three), indicating its  
 577 suitability for practical scenarios with a good level of security and accuracy. Future research  
 578 directions that could lead to more accurate user identification, gender classification and  
 579 authentication are as follows. End-to-end learning approach can be applied to the whole network  
 580 with a sufficiently large database and more biometrics. A model that works well with more biometrics  
 581 can achieve better performance in the missing modal situation since the remaining modals can  
 582 complement the functionality of the missing modal. It should be noted that the technique used for  
 583 the multimodal data fusion in the proposed model was to simply concatenate the multimodal  
 584 features, and this can be improved further by using an attention model to select the most suitable  
 585 modality or feature that is present in the sample.  
 586

## 587 Acknowledgement

588 This work is supported in part by the Center for Cyber-Physical Systems, Khalifa University, under Grant  
 589 Number 8474000137-RC1-C2PS-T3. The authors declare no conflict of interest.  
 590

## 591 References

- 592 1. Wang, Y.; Agrafioti, F.; Hatzinakos, D.; Plataniotis, K.N. Analysis of human electrocardiogram for biometric  
 593 recognition. *EURASIP journal on Advances in Signal Processing* **2007**, *2008*, 148658.
- 594 2. Coutinho, D.P.; Fred, A.L.; Figueiredo, M.A. One-lead ECG-based personal identification using Ziv-Merhav cross  
 595 parsing. 2010 20th International Conference on Pattern Recognition. IEEE, 2010, pp. 3858–3861.
- 596 3. Lee, J.; Chee, Y.; Kim, I. Personal identification based on vectorcardiogram derived from limb leads  
 597 electrocardiogram. *Journal of Applied Mathematics* **2012**, *2012*.
- 598 4. Li, M.; Narayanan, S. Robust ECG biometrics by fusing temporal and cepstral information. 2010 20th  
 599 International Conference on Pattern Recognition. IEEE, 2010, pp. 1326–1329.
- 600 5. Fang, S.C.; Chan, H.L. Human identification by quantifying similarity and dissimilarity in electrocardiogram  
 601 phase space. *Pattern Recognition* **2009**, *42*, 1824–1831.
- 602 6. Kim, J.; Lee, K.B.; Hong, S.G. ECG-based biometric authentication using random forest. *Journal of the Institute of*  
 603 *Electronics and Information Engineers* **2017**, *54*, 100–105.
- 604 7. Plataniotis, K.N.; Hatzinakos, D.; Lee, J.K. ECG biometric recognition without fiducial detection. 2006 Biometrics  
 605 symposium: Special session on research at the biometric consortium conference. IEEE, 2006, pp. 1–6.
- 606 8. Gang, G.W.; Min, C.H.; Kim, T.S. Development of Single Channel ECG Signal Based Biometrics System. *Journal of*  
 607 *the Institute of Electronics Engineers of Korea CI* **2012**, *49*, 1–7.
- 608 9. Odinaka, I.; Lai, P.H.; Kaplan, A.D.; O'Sullivan, J.A.; Sirevaag, E.J.; Rohrbough, J.W. ECG biometric recognition: A  
 609 comparative analysis. *IEEE Transactions on Information Forensics and Security* **2012**, *7*, 1812–1824.
- 610 10. Kim, S.K.; Yeun, C.Y.; Damiani, E.; Lo, N.W. A machine learning framework for biometric authentication using  
 611 electrocardiogram. *IEEE Access* **2019**, *7*, 94858–94868.
- 612 11. Al Alkeem, E.; Kim, S.K.; Yeun, C.Y.; Zemerly, M.J.; Poon, K.F.; Gianini, G.; Yoo, P.D. An enhanced  
 613 electrocardiogram biometric authentication system using machine learning. *IEEE Access* **2019**, *7*, 123069–  
 614 123075.
- 615 12. Sun, L.; Lu, Y.; Yang, K.; Li, S. ECG analysis using multiple instance learning for myocardial infarction detection.  
 616 *IEEE transactions on biomedical engineering* **2012**, *59*, 3348–3356.

- 617 13. Krizhevsky, A.; Sutskever, I.; Hinton, G.E. Imagenet classification with deep convolutional neural networks.  
618 *Communications of the ACM* **2017**, *60*, 84–90.
- 619 14. Hinton, G.; Deng, L.; Yu, D.; Dahl, G.E.; Mohamed, A.R.; Jaitly, N.; Senior, A.; Vanhoucke, V.; Nguyen, P.; Sainath,  
620 T.N.; others. Deep neural networks for acoustic modeling in speech recognition: The shared views of four  
621 research groups. *IEEE Signal processing magazine* **2012**, *29*, 82–97.
- 622 15. Isin, A.; Ozdalili, S. Cardiac arrhythmia detection using deep learning. *Procedia computer science* **2017**, *120*,  
623 268–275.
- 624 16. Labati, R.D.; Muñoz, E.; Piuri, V.; Sassi, R.; Scotti, F. Deep-ECG: convolutional neural networks for ECG biometric  
625 recognition. *Pattern Recognition Letters* **2019**, *126*, 78–85.
- 626 17. Velayudhan, A.; Peter, S. Noise analysis and different denoising techniques of ECG signal-a survey. *IOSR journal*  
627 *of electronics and communication engineering* **2016**, *3*, 641–644.
- 628 18. Biel, L.; Pettersson, O.; Philipson, L.; Wide, P. ECG analysis: a new approach in human identification. *IEEE*  
629 *Transactions on Instrumentation and Measurement* **2001**, *50*, 808–812.
- 630 19. Israel, S.A.; Irvine, J.M.; Cheng, A.; Wiederhold, M.D.; Wiederhold, B.K. ECG to identify individuals. *Pattern*  
631 *recognition* **2005**, *38*, 133–142.
- 632 20. Kim, K.S.; Yoon, T.H.; Lee, J.W.; Kim, D.J.; Koo, H.S. A robust human identification by normalized time-domain  
633 features of electrocardiogram. 2005 IEEE Engineering in Medicine and Biology 27th Annual Conference. IEEE,  
634 2006, pp. 1114–1117.
- 635 21. Gahi, Y.; Lamrani, M.; Zoglat, A.; Guennoun, M.; Kapralos, B.; El-Khatib, K. Biometric identification system based  
636 on electrocardiogram data. 2008 New Technologies, Mobility and Security. IEEE, 2008, pp. 1–5. Song, H.K.;
- 637 22. AlAlkeem, E.; Yun, J.; Kim, T.H.; Yoo, H.; Heo, D.; Chae, M.; Yeun, C.Y. Deep user identification model with multiple  
638 biometric data. *BMC bioinformatics* **2020**, *21*, 1–11.
- 639 23. Israel, S.A.; Scruggs, W.T.; Worek, W.J.; Irvine, J.M. Fusing face and ECG for personal identification. 32nd Applied  
640 Imagery Pattern Recognition Workshop, 2003. Proceedings. IEEE, 2003, pp. 226–231.
- 641 24. BE, M.; M Abhishek, A.; KR, V.; M Patnaik, L.; others. Multimodal Biometric Authentication using ECG and  
642 Fingerprint. *IJCA*, 2015, Vol. 111, pp. 33–39.
- 643 25. Boumbarov, O.; Velchev, Y.; Tonchev, K.; Paliy, I.; Chetty, G. Face and ECG based multi-modal biometric  
644 authentication. In *Advanced biometric technologies*; InTech, 2011.
- 645 26. Zokaee, S.; Faez, K. Human identification based on ECG and palmprint. *International Journal of Electrical and*  
646 *Computer Engineering* **2012**, *2*, 261.
- 647 27. Yaacoubi, C., Besrou, R., & Lachiri, Z. A multimodal biometric identification system based on ECG and  
648 PPG signals. *Proceedings of the 2nd International Conference on Digital Tools & Uses Congress 2020*, pp. 1-6.
- 649 28. Fan, J.; Cao, X.; Wang, Q.; Yap, P.T.; Shen, D. Adversarial learning for mono-or multi-modal registration. *Medical*  
650 *image analysis* **2019**, *58*, 101545.
- 651 29. Zhou, T.; Liu, M.; Thung, K.H.; Shen, D. Latent representation learning for Alzheimer's disease diagnosis with  
652 incomplete multi-modality neuroimaging and genetic data. *IEEE transactions on medical imaging* **2019**, *38*,  
653 2411–2422.
- 654 30. Zhou, T.; Thung, K.H.; Liu, M.; Shi, F.; Zhang, C.; Shen, D. Multi-modal latent space inducing ensemble SVM  
655 classifier for early dementia diagnosis with neuroimaging data. *Medical Image Analysis* **2020**, *60*, 101630.
- 656 31. Gavrilova, M.L.; Monwar, M. *Multimodal biometrics and intelligent image processing for security systems*;  
657 Information Science Reference, 2013.
- 658 32. Chergui, O.; Bendjenna, H.; Meraoumia, A.; Chitroub, S. Combining palmprint & finger-knuckle-print for user  
659 identification. 2016 International Conference on Information Technology for Organizations Development  
660 (IT4OD). IEEE, 2016, pp. 1–5.
- 661 33. Huo, G.; Liu, Y.; Zhu, X.; Dong, H.; He, F. Face-iris multimodal biometric scheme based on feature level fusion.  
662 *Journal of Electronic Imaging* **2015**, *24*, 063020.
- 663 34. Snelick, R.; Uludag, U.; Mink, A.; Indovina, M.; Jain, A. Large-scale evaluation of multimodal biometric  
664 authentication using state-of-the-art systems. *IEEE transactions on pattern analysis and machine intelligence*  
665 **2005**, *27*, 450–455.
- 666 35. Ross, A.A.; Nandakumar, K.; Jain, A.K. *Handbook of multibiometrics*; Vol. 6, Springer Science & Business Media,  
667 2006.
- 668 36. Ross, A.; Jain, A. Information fusion in biometrics. *Pattern recognition letters* **2003**, *24*, 2115–2125.
- 669 37. Ross, A.A.; Govindarajan, R. Feature level fusion of hand and face biometrics. Biometric technology for human  
670 identification II. International Society for Optics and Photonics, 2005, Vol. 5779, pp. 196–204.

- 671 38. Rattani, A.; Kisku, D.R.; Bicego, M.; Tistarelli, M. Feature level fusion of face and fingerprint biometrics. 2007  
672 First IEEE International Conference on Biometrics: Theory, Applications, and Systems. IEEE, 2007, pp. 1–6.
- 673 39. Kittler, J.; Hatef, M.; Duin, R.P.; Matas, J. On combining classifiers. *IEEE transactions on pattern analysis and*  
674 *machine intelligence* **1998**, *20*, 226–239.
- 675 40. Duda, R.O.; Hart, P.E.; Stork, D.G. *Pattern classification*; John Wiley & Sons, 2012.
- 676 41. Lam, L.; Suen, S. Application of majority voting to pattern recognition: an analysis of its behavior and  
677 performance. *IEEE Transactions on Systems, Man, and Cybernetics-Part A: Systems and Humans* **1997**, *27*, 553–  
678 568.
- 679 42. Daugman, J. Biometric decision landscapes. Technical report, University of Cambridge, Computer Laboratory,  
680 2000.
- 681 43. Rautiainen, M.; Seppanen, T. Comparison of visual features and fusion techniques in automatic detection of  
682 concepts from news video. 2005 IEEE International Conference on Multimedia and Expo. IEEE, 2005, pp. 932–  
683 935.
- 684 44. Dummett, M.A.; others. *Principles of electoral reform*; Oxford University Press Oxford, 1997.
- 685 45. Ho, T.K.; Hull, J.J.; Srihari, S.N. Decision combination in multiple classifier systems. *IEEE transactions on pattern*  
686 *analysis and machine intelligence* **1994**, *16*, 66–75.
- 687 46. Aslam, J.A.; Montague, M. Models for metasearch. Proceedings of the 24th annual international ACM SIGIR  
688 conference on Research and development in information retrieval, 2001, pp. 276–284.
- 689 47. Aslam, J.A.; Montague, M. Bayes optimal metasearch: a probabilistic model for combining the results of multiple  
690 retrieval systems. Proceedings of the 23rd annual international ACM SIGIR conference on Research and  
691 development in information retrieval, 2000, pp. 379–381.
- 692 48. Melnik, O.; Vardi, Y.; Zhang, C.H. Mixed group ranks: Preference and confidence in classifier combination. *IEEE*  
693 *Transactions on Pattern Analysis and Machine Intelligence* **2004**, *26*, 973–981.
- 694 49. Ergin, S.; Uysal, A.K.; Gunal, E.S.; Gunal, S.; Gulmezoglu, M.B. ECG based biometric authentication using ensemble  
695 of features. 2014 9th Iberian Conference on Information Systems and Technologies (CISTI). IEEE, 2014, pp. 1–  
696 6.
- 697 50. Caruana, R. Multitask Learning: A Knowledge-Based Source of Inductive Bias ICML. *Google Scholar Google*  
698 *Scholar Digital Library Digital Library* **1993**.
- 699 51. Ruder, S. An overview of multi-task learning in deep neural networks. *arXiv preprint arXiv:1706.05098* **2017**.
- 700 52. Ji, J.; Chen, X.; Luo, C.; Li, P. A deep multi-task learning approach for ECG data analysis. 2018 IEEE EMBS  
701 International Conference on Biomedical & Health Informatics (BHI). IEEE, 2018, pp. 124–127.
- 702 53. Lin, Y.; Lv, F.; Zhu, S.; Yang, M.; Cour, T.; Yu, K.; Cao, L.; Huang, T. Large-scale image classification: Fast feature  
703 extraction and SVM training. CVPR 2011. IEEE, 2011, pp. 1689–1696.
- 704 54. Szegedy, C.; Ioffe, S.; Vanhoucke, V.; Alemi, A. Inception-v4, inception-resnet and the impact of residual  
705 connections on learning. *arXiv preprint arXiv:1602.07261* **2016**.
- 706 55. Salloum, R.; Kuo, C.C.J. ECG-based biometrics using recurrent neural networks. 2017 IEEE International  
707 Conference on Acoustics, Speech and Signal Processing (ICASSP). IEEE, 2017, pp. 2062–2066.
- 708 56. Kingma, D.P.; Ba, J. Adam: A method for stochastic optimization. *arXiv preprint arXiv:1412.6980* **2014**.
- 709 57. Duchi, J.; Hazan, E.; Singer, Y. Adaptive subgradient methods for online learning and stochastic optimization.  
710 *Journal of machine learning research* **2011**, *12*.
- 711 58. Hinton, G.; Srivastava, N.; Swersky, K. Neural networks for machine learning. *Coursera, video lectures* **2012**, *264*.
- 712 59. Goldberger, A.L.; Amaral, L.A.; Glass, L.; Hausdorff, J.M.; Ivanov, P.C.; Mark, R.G.; Mietus, J.E.; Moody, G.B.; Peng,  
713 C.K.; Stanley, H.E. PhysioBank, PhysioToolkit, and PhysioNet: components of a new research resource for  
714 complex physiologic signals. *circulation* **2000**, *101*, e215–e220.
- 715 60. Lugovaya, T. Biometric human identification based on electrocardiogram. *Master's thesis, Faculty of Computing*  
716 *Technologies and Informatics, Electrotechnical University 'LETI', Saint-Petersburg, Russian Federation* **2005**.
- 717 61. Boussejot, R.; Kreiseler, D.; Schnabel, A. Nutzung der EKG-Signaldatenbank CARDIODAT der PTB über das  
718 Internet. *Biomedizinische Technik/Biomedical Engineering* **1995**, *40*, 317–318.
- 719 62. Hond, D.; Spacek, L. Distinctive Descriptions for Face Processing. BMVC, 1997, number 0.2, pp. 0–4.
- 720 63. Cappelli, R.; Ferrara, M.; Franco, A.; Maltoni, D. Fingerprint verification competition 2006. *Biometric Technology*  
721 *Today* **2007**, *15*, 7–9.
- 722 64. Jain, A.K.; Hong, L.; Pankanti, S.; Bolle, R. An identity-authentication system using fingerprints. *Proceedings of*  
723 *the IEEE* **1997**, *85*, 1365–1388.

- 724 65. El-Sayed, A. Multi-biometric systems: a state of the art survey and research directions. *IJACSA) International*  
725 *Journal of Advanced Computer Science and Applications* **2015**, 6.
- 726 66. Vishi, K.; Mavroeidis, V. An evaluation of score level fusion approaches for fingerprint and finger-vein  
727 biometrics. *arXiv preprint arXiv:1805.10666* **2018**.
- 728